Kidney360

# COVID-19–Associated Nephropathy Includes Tubular Necrosis and Capillary Congestion, with Evidence of SARS-CoV-2 in the Nephron

*Antoine Bouquegneau,[1] Pauline Erpicum,[1,2] Stéphanie Grosch,[1,3] Lionel Habran,[3] Olivier Hougrand,[3] Justine Huart,[1,2] Jean-Marie Krzesinski,[1,2] Benoît Misset,[4] Marie-Pierre Hayette,[5] Philippe Delvenne,[3] Christophe Bovy,[1,3] Dominik Kylies,[6] Tobias B. Huber,[6] Victor G. Puelles[6], Pierre Delanaye[1,7] and François Jouret[1,2]*

## Key Points

- The pathophysiology of SARS-CoV-2–induced AKI is poorly understood and may involve direct renal lesions by the virus itself.
- We demonstrated acute tubular necrosis of variable severity, with unusual congestion of the glomerular and peritubular capillaries.
- A positive signal for SARS-CoV-2 was detected at both RNA and protein levels in various kidney compartments.

## Abstract

**Background** Kidney damage has been reported in patients with COVID-19. Despite numerous reports about COVID-19–associated nephropathy, the factual presence of the SARS-CoV-2 in the renal parenchyma remains controversial.

**Methods** We consecutively performed 16 immediate (≤3 hours) *postmortem* renal biopsies in patients diagnosed with COVID-19. Kidney samples from five patients who died from sepsis not related to COVID-19 were used as controls. Samples were methodically evaluated by three pathologists. Virus detection in the renal parenchyma was performed in all samples by bulk RNA RT-PCR (E and N1/N2 genes), immunostaining (2019-nCOV N-Protein), fluorescence *in situ* hybridization (nCoV2019-S), and electron microscopy.

**Results** The mean age of our COVID-19 cohort was 68.2±12.8 years, most of whom were male (69%). Proteinuria was observed in 53% of patients, whereas AKI occurred in 60% of patients. Acute tubular necrosis of variable severity was found in all patients, with no tubular or interstitial inflammation. There was no difference in acute tubular necrosis severity between the patients with COVID-19 versus controls. Congestion in glomerular and peritubular capillaries was respectively observed in 56% and 88% of patients with COVID-19, compared with 20% of controls, with no evidence of thrombi. The 2019-nCOV N-Protein was detected in proximal tubules and at the basolateral pole of scattered cells of the distal tubules in nine out of 16 patients. *In situ* hybridization confirmed these findings in six out of 16 patients. RT-PCR of kidney total RNA detected SARS-CoV-2 E and N1/N2 genes in one patient. Electron microscopy did not show typical viral inclusions.

**Conclusions** Our immediate *postmortem* kidney samples from patients with COVID-19 highlight a congestive pattern of AKI, with no significant glomerular or interstitial inflammation. Immunostaining and *in situ* hybridization suggest SARS-CoV-2 is present in various segments of the nephron.

*KIDNEY360* 2: 639–652, 2021. doi: https://doi.org/10.34067/KID.0006992020

## Introduction

A novel coronavirus named severe acute respiratory syndrome coronavirus 2 (SARS-CoV-2) was isolated in December 2019 in China (1). This virus causes coronavirusdisease 2019 (COVID-19) (1,2), which is characterizedby a diffuse alveolar damage leading to an acute respiratory distress syndrome (ARDS) (3,4). Organs other than the lungs may be affected, including the kidneys (3,5–7). The earliest report showed that proteinuria and hematuria were detected at hospital admission in 44% and 27% of patients with COVID-19, whereas approximately 15% of them presented with elevated levels of serum

[1]Department of Nephrology, Dialysis and Transplantation, ULiège Academic Hospital, Liège, Belgium
[2]Department Groupe Interdisciplinaire de Géno-protéomique Appliquée, Cardiovascular Sciences, ULiège, Liège, Belgium
[3]Department of Pathology, ULiège Academic Hospital, Liège, Belgium
[4]Department of Intensive Care, ULiège Academic Hospital, Liège, Belgium
[5]Department of Clinical Microbiology, ULiège Academic Hospital, Liège, Belgium
[6]III. Department of Medicine, University Medical Center Hamburg-Eppendorf, Hamburg, Germany
[7]Department of Nephrology-Dialysis-Apheresis, University Hospital Caremeau, Nimes, France

**Correspondence:** Antoine Bouquegneau, CHU de Liège, Sart Tilman Hospital, Avenue de l'Hôpital, 4000, Liège, Belgium. Email: antoine.bouquegneau@chuliege.be

creatinine and/or BUN (5). Proteinuria characterization suggests a tubular origin (8). AKI has been identified as an independent risk factor for in-hospital mortality (3–5,9). In the United States, AKI among hospitalized patients with COVID-19 may range between 28% and 46% (10), with a high risk of in-hospital mortality (11).

The pathophysiology of COVID-19–associated AKI is poorly understood and may involve (*1*) the cytokine release syndrome (12,13); (*2*) the hypercoagulable state leading to acute tubular necrosis (ATN) and cortical necrosis (14,15); and/or (*3*) direct renal lesions by the virus itself (7,16–18). In addition, the hemodynamic instability induced by SARS-CoV-2 infection may cause an ischemic ATN *per se*, as typically observed in patients with sepsis. Receptors for SARS-CoV-2 include angiotensin-converting enzyme 2 (ACE2) (16,19), and CD147 (20) and GRP78 (19). ACE2 is largely expressed at the surface of respiratory cells, and might be more involved in SARS-CoV-2 infection compared with other receptors. Renal tubular cells and podocytes also express ACE2 on the luminal side of their plasma membrane (21,22). However, the factual presence of the virus in the urinary system remains largely debated (6,9,23–29).

In this study, we prospectively aimed to (*1*) describe the histologic findings in consecutive *postmortem* kidney biopsies of patients with COVID-19 in correlation with their medical history, and (*2*) assess whether the SARS-CoV-2 virus is segmentally detectable in the nephron.

## Materials and Methods

### Patients

Kidney biopsies were performed in adult patients deceased from COVID-19 inside and outside the intensive care unit (ICU) between March 30, 2020 and June 4, 2020 at ULiège Academic Hospital. None of these samples have been used in whole or in part in previous reports. Our study was approved by the Ethics Committee of ULiège Academic Hospital (B707201215598–020/119) in agreement with the ethical standards of Declaration of Helsinki and the Belgian law about immediate autopsies (which stipulates that autopsies or biopsies may be performed without the written informed consent of the patient or family in case of "urgent medical and/or scientific need," such as a novel infectious disease). Note that relatives of the patients included in this study were systematically informed before the biopsy procedure. Patients with and without AKI were eligible. The SARS-CoV-2 reverse-transcriptase PCR (RT-PCR) was performed on nasopharyngeal swabs using the Cobas SARS-CoV-2 assay (cobas 6800; Roche), which targets E and ORF1ab genes (30,31). A control group of five patients without COVID-19 was used to evaluate the COVID-19–induced histologic lesions. Four patients with an *antemortem* diagnosis of sepsis and/or ARDS, who underwent an autopsy within 24 hours, were identified in the database of the Department of Pathology (*i.e.,* patients R1–R4). One control patient died from pulmonary sepsis not related to COVID-19 in ICU during the present prospective recruitment (patient P1) and was PCR negative for SARS-CoV-2. The immunocompromised status was defined as having a history of cancer or active cancer, transplantation, HIV infection, type 1 diabetes, or inflammatory disease.

### Kidney Biopsy

Percutaneous kidney biopsy was performed under ultrasound guidance, *via* a disposable 16-G biopsy needle (ISTOCORE) targeting the lower pole of the kidney (either left or right). The patient was in a prone position. All biopsies were carried out by the same investigator (A.B.) within a maximum period of 3 hours *postmortem*. Three samples (each approximately 15 mm long by 3 mm wide) were collected. The first sample was immediately fixed in 10% paraformaldehyde for 48 hours; the second sample was immersed in 4% glutaraldehyde; the third sample was snap frozen in liquid nitrogen. Conventional protective measures against viral spread were followed, including protection of the airways during the procedures and the fixation of tissue specimens for 48 hours before handling. The renal paraffin blocks of control patients R1–R4 were retrieved for the archives and processed in parallel with the COVID-19 samples.

### Clinical, Biologic, and Radiologic Parameters

Clinical data were collected from medical records and anonymized: age, weight, height, body mass index, history of hypertension, history of diabetes, active or previous cancer, active smoking, and CKD. All biologic data were obtained from the same laboratory. Blood levels of C-reactive protein, procalcitonin, creatinine, lactate dehydrogenase, and potassium were determined using the Abbott Alinity instrument. Lymphocytes and platelet measurement were obtained using the Sysmex SE-9000 Hematology analyzer. Plasma D-Dimer levels were measured with the Innovance D-Dimer kit on the automated Siemens CS5100. The number of red blood cells in the urine was automatically evaluated using a sediMAX. The eGFR was calculated using the CKD-epidemiology equation (32). Proteinuria was staged according to the kidney disease improved global outcomes (KDIGO) staging system (33). AKI definition and stages were defined according to the KDIGO guidelines (34). The incidence of a $\geq$30% decrease of eGFR during hospitalization was also assessed. The severity scoring of COVID-19 pneumonia was on the basis of the percentage of the lungs involved on a thorax computed tomography (CT) scanner, as reported by the radiologists in charge: minor if $<$10%; mild between 10% and 50%; and severe if $>$50% of lung involvement (35).

### Histologic Analyses

*Light Microscopy*

All biopsies were prepared using standard techniques. A conventional description by light microscopy on the basis of routine colorations, namely hematoxylin and eosin, Periodic Acid–Shiff, Jones silver coloration, and Masson Trichrome, was performed independently by three pathologists (S.G., C.B., P.E.) blinded for the medical history, according to an *a priori* defined criteria listed in Supplemental Table 1. Briefly, tissue sections were systematically scored for (*1*) proliferation, sclerosis, and ischemia in the glomeruli; (*2*) tubulitis, cell vacuolization, necrosis, and atrophy in the tubules; (*3*) edema, inflammation, and fibrosis in the interstitium; and (*4*) congestion, thrombi, endothelial cell swelling, arteriolar hyalinosis, and peritubular capillaritis in the vasculature (36).

*Immunohistochemical Studies*

Immunohistochemistry was performed on formalin-fixed paraffin-embedded (FFPE) samples. Immunostaining for ACE2 (SN0754; GeneTex), $Na^+/Cl^-$ cotransporter (NCC, rabbit anti-NCC ab3553; Merck), CD10 (790–4506; VENTANA), and CD31 (760–4378; VENTANA) was performed on all samples. In patients with erythrocyte aggregation in the capillaries, the presence of thrombi was determined using immunohistochemistry for CD61 (platelet marker; Sigma Aldrich), CD42b (platelet marker;

BioSB), and Martius Blue Scarlet staining (fibrin marker, RRSK2–500; Atom Scientific). The conventional negative and positive controls for each technique were adequately used.

*Virus Detection*

Immunostaining for the nucleocapsid of SARS-CoV-2 was performed on all patients using 2019-nCoV N-Protein (NP) rabbit polyclonal antibody (A20016; ABclonal) (25,37). Sections of lungs from guinea pigs infected by SARS-CoV-2 were used as positive controls. Briefly, FFPE tissue sections were subjected to $H_2O$-based antigen retrieval. Endogenous peroxidase activity was blocked with 3% hydrogen peroxide. Nonspecific binding was constrained by incubation with Protein Block Serum Free. Specimens were then incubated for 60 minutes at room temperature with primary antibody (1/100). After washing, sections were incubated for 30 minutes with Polyview Plus AP anti-rabbit secondary antibody (ENZ-ACC110–0150; Enzo). Immunoreactivity was detected using AP (ADI-950-I41–0030; Enzo), and sections were counterstained with hematoxylin and eosin. The extent of 2019-nCoV NP positivity was semiquantitatively scored on the Banff classification for definitive polyomavirus nephropathy (38). Total RNA extraction from FFPE kidney sections was performed with a Maxwell 16 LEV RNA FFPE kit (AS1260; Promega) (39). RT-PCR was performed on LC480 thermocycler (Roche) using the Viral RNA UM Master Mix (Qiagen) after confirmation of the integrity of the human genetic material (B2M and RNAseP genes). The E and N1/N2 genes of SARS-CoV-2 were targeted using the following cycling conditions: 50°C for 10 minutes, 95°C for 2 minutes, and 40 cycles at 95°C for 5 seconds, 58°C for 30 seconds (30).

*Fluorescence In Situ Hybridization for SARS-CoV-2 RNA Spatial Identification*

*In situ* hybridization (ISH) was performed on FFPE human kidney samples using RNAscope technology as previously described (40), in accordance with the directions from Advanced Cell Diagnostics. The RNAscope V-nCoV2019-S probe from Advanced Cell Diagnostics was used as the target probe to detect the SARS-CoV-2 S gene encoding the viral spike protein. Fluorescent labeling of the target probe was performed using OPAL 690 dye from Akoya Biosciences (FP1497001KT, dilution 1:1000). RNAscope 3-plex positive- and negative control probe mixes from Advanced Cell Diagnostics were used to ascertain RNA quality, and to exclude false-positive signaling. Fluorescent labeling of the positive- and negative-control probe mix were performed using OPAL 520 and 690 dyes from Akoya Biosciences (FP1487001KT, FP1488001KT, and FP1497001KT, respectively, all dilutions 1:1500). Nuclear costaining was performed using the DAPI solution from Advanced Cell Diagnostics. Immunostaining with Lotus tetragonolobus lectin (LTL) was performed in the same sections after completing the RNAscope protocol. The primary antibody specific to LTL was applied for 12 hours at 4°C (B-1325–2, dilution 1:200; Vectorlabs). The secondary antibody Alexa Fluor 555 streptavidin conjugate from ThermoFisher Scientific (S32355, dilution 1:400) was applied for 60 minutes at 4°C. Epifluorescence imaging was performed using the Thunder Imager 3D Live Cell and 3D Cell Culture from Leica Microsystems.

*Electron Microscopy*

Tissues were fixed at 4°C in 4% glutaraldehyde in phosphate buffer at pH 7.4, postfixed in 1% osmium tetrooxide for 1 hour at 4°C. Then they were dehydrated in graded (70%, 90%, 100%) ethanol solutions and propylene oxide, embedded in Epon, and hardened at 60°C. Semithin sections were stained with 0.5% toluidine blue and examined by light microscopy. Ultrathin sections (80 nm) were stained with uranyl acetate and lead citrate. These sections were examined using a Zeiss EM 910 transmission electron microscope (60 kV).

### Statistical Analyses

Data were expressed as mean (minimum value; maximum value) when the distribution was normal, and as median with interquartile range (IQR) (quartile 1; quartile 3) if not. Normality was assessed by the Shapiro-Wilk test. Categorical variables were expressed as percentages. Statistical difference was evaluated by a *t* test in the case of normally distributed variables or by a rank test where continuous variables were not normally distributed and by Fisher's exact test for categorical variables. The Spearman rank-order correlation coefficient was used to measure the strength and direction of association between two variables measured on an ordinal or continuous scale. Analyses were conducted using STATA (version 15; StataCorp, College Station, TX).

## Results

### Characteristics of the Population

All of the 16 White patients showed a positive RT-PCR–based amplification of SARS-CoV-2 using nasopharyngeal swab before death (basically at hospital admission) and presented with thoracic CT compatible with COVID-19 pneumonia. The median length between SARS-CoV-2 positivity through nasopharyngeal sampling and death was 14 days (IQR, 7.5–25.5). Their clinical and laboratory characteristics are summarized in Table 1. For informational purposes, Supplemental Table 2 distinguishes the patients on the basis of their location at the time of death, namely, inside versus outside the ICU. Ten patients (63%) died in the ICU. The mean age of our 16-patient cohort was 68.2±12.8 years, with a male predominance (69%). Patients in the ICU were significantly younger ($P=0.007$). The body mass index reached 30.7±6.1 kg/m$^2$. Hypertension, diabetes, and CKD were present in 63%, 56%, and 43% of patients, respectively (Table 1). Our cohort included two heart transplant recipients (patients 7 and 11), and one patient with a history of prostate cancer (patient 6). The median length of hospital stay was 14 days (IQR, 7.5–25.5), with a significantly longer stay for patients in ICU (Supplemental Table 2). Lymphocyte count was at the lower level of the norm, whereas blood levels of C-reactive protein, fibrinogen, D-dimer, and lactate dehydrogenase were above the normal ranges at hospital admission (Table 1 and Supplemental Table 2). Most of the patients in the ICU had a more severe form of COVID-19, with a higher prevalence (60%) of severe CT-based score compared with patients not in the ICU (17%) at admission. AKI concerned 60% of patients during hospitalization, with 53% showing stage 3 proteinuria at admission and a median proteinuria of 580 (320; 830) mg/g urine creatinine (Table 1). During their hospitalization, patients in the ICU developed a 30% decrease in eGFR more frequently than patients not in the ICU (Supplemental Table 2). Three patients required RRT. The clinical and biologic characteristics of the control patients ($n=5$) are summarized in Supplemental Table 3. The cause of death was related to sepsis and ARDS in 81% of patients.

### Histologic Findings

Table 2 summarizes the most relevant pattern of renal lesions observed by light microscopy in all patients, including both

**Table 1. Clinical and biologic characteristics of the severe acute respiratory syndrome coronavirus 2–infected group**

| Characteristic | Result |
|---|---|
| **Clinical** | |
| Age (yr) mean (min; max) (*n*=16) | 68.2 (49; 95) |
| Women % (*n*=16) | 31.3 |
| Body mass index (kg/m$^2$) mean (min; max) (*n*=16) | 30.7 (20.7; 39.6) |
| **Medical history** | |
| Hypertension % (*n*=16) | 62.5 |
| Diabetes % (*n*=16) | 56.3 |
| CKD % (*n*=14) | 42.9 |
| Active cancer or history % (*n*=14) | 12.5 |
| Cardiovascular disease % (*n*=16) | 43.8 |
| Immunocompromise status % (*n*=16) | 25 |
| Asthma/COPD % (*n*=16) | 0 |
| Nonsmoker % (*n*=14) | 78.6 |
| RAAS inhibitors drugs % (*n*=16) | 50 |
| Hydroxychloroquine used during hospitalization % (*n*=16) | 87.5 |
| Contrast products injection during hospitalization % (*n*=16) | 18.8 |
| Antiplatelets used before hospitalization % (*n*=16) | 43.8 |
| Anticoagulation during hospitalization % (*n*=16) | 75 |
| Hospital stay length (d) median (IQR) (*n*=16) | 14 (7.5–22.5) |
| **Severity** | |
| ICU admission % (*n*=16) | 62.5 |
| Thorax CT scanner staging % (*n*=16) | |
| Minor (<10%) | 18.8 |
| Mild (10%–50%) | 37.5 |
| Severe (>50%) | 43.7 |
| Renal severity | |
| AKI % (*n*=16) | 62.5 |
| CVVH initiation during hospitalization % (*n*=16) | 18.5 |
| 30% decrease of eGFR during hospitalization % (*n*=16) | 50 |
| Proteinuria at D0 >500 mg/g of urine creatinine % (*n*=15) | 53.3 |
| Hematuria at D0 % (*n*=13) | 53.8 |
| **Biologic** | |
| ABO group % (*n*=14) | |
| A–B–AB–O | 64.3–14.3–0 –21.4 |
| Lymphocytes at D0 (/mm$^3$) median (IQR) (*n*=16) | 720 (520–1440) |
| Lymphocytes at end of hospitalization (/mm$^3$) median (IQR) (*n*=15) | 970 (530–1280)[a] |
| Platelet at D0 (×1000/mm$^3$) mean (min; max) (*n*=16) | 211.4 (79; 417) |
| Platelet at end of hospitalization (×1000/mm$^3$) mean (min; max) (*n*=15) | 230.3 (26; 457)[a] |
| C-reactive protein at D0 (mg/L) mean (min; max) (*n*=16) | 166.5 (4.4; 382.4) |
| C-reactive protein at end of hospitalization (mg/L) mean (min; max) (*n*=15) | 195.5 (3.8; 311.9)[a] |
| Fibrinogen (g/L) at D0 median (IQR) (*n*=16) | 7.18 (4.83–7.72) |
| Fibrinogen (g/L) at end of hospitalization, median (IQR) (*n*=15) | 6.96 (5.01; 7.86)[a] |
| Procalcitonin at D0 (μg/L) median (IQR) (*n*=13) | 0.33 (0.16–0.83) |
| D-dimer at D0 (μg/L) mean (min; max) (*n*=11) | 1309.5 (329; 2991) |
| LDH at D0 (U/L) mean (min; max) (*n*=16) | 532.8 (195; 881) |
| CPK at D0 (U/L) median (IQR) (*n*=16) | 286.5 (181.5–445) |
| eGFR (before hospitalization) (*n*=13) | |
| 60–90 ml/min per 1,73 m$^2$ % | 46.2 |

**Table 1. (Continued)**

| Characteristic | Result |
|---|---|
| <60ml/min per 1,73 $m^2$ % | 23.1 |
| <30 ml/min per 1,73 $m^2$ % | 0 |
| Serum creatinine at D0 (mg/dl) median (IQR) (*n*=16) | 1.07 (0.83–1.27) |
| Serum creatinine at end of hospitalization (mg/dl) median (IQR) (*n*=16) | 0.96 (0.68–1.62)[a] |
| Potassium at D0 (mmol/L) mean (min; max) (*n*=16) | 4.16 (3.55; 4.63) |
| Proteinuria at D0 (mg/g of urine creatinine), median (IQR) (*n*=15) proteinuria at D7 (mg/g of urine creatinine) median (IQR) (*n*=10) | 580 (320–830)<br>650 (400–1520)[b] |
| **Delay biopsy (*n*=16)** | |
| <60 (min) % | 62.5 |
| 60–120 (min) % | 12.5 |
| 120–180 (min) % | 25 |

COPD, chronic obstructive pulmonary disease; D0, day 0 of hospital admission; D7, day 7 after hospital admission; RAAS, renin angiotensin aldosterone system; IQR, interquartile range; ICU, intensive care unit; CT, computed tomography; CVVH, continuous venovenous hemofiltration; LDH, lactate dehydrogenase; CPK, creatinine phospho-kinase.

aNo statistical difference observed between D0 and the end of hospitalization.

bNo statistical difference observed between D0 and D7.

COVID-19 ($n=16$) and control ($n=5$) groups. The biopsies had a median of 31 (18–49) glomeruli, with a median of 12 (2–17) sclerotic glomeruli in the COVID-19 group. The P1 sample showed 33 glomeruli with no sclerosis, whereas the archival R1–R4 tissues had ≥500 glomeruli. All patients with COVID-19 and controls demonstrated ATN lesions to a variable extent, which were mainly characterized by tubular vacuolization ($n=12$ out of 21), loss of proximal tubule (PT) brush border ($n=20$ out of 21), cell shedding ($n=12$ out of 21), and/or apoptosis ($n=17$ out of 21) (Figure 1). ATN severity was not different between COVID-19 versus control samples. No tubulitis or interstitial infiltrate was observed in either group. In our study, three patients (5, 7, and 11) had been exposed to intravenous (IV) contrast during the hospitalization, and two patients (7 and 11) were treated by calcineurin inhibitors as a long-life therapy for heart transplantation. No patient received IV Ig, nonsteroidal anti-inflammatory drugs, or vitamin C during the hospitalization. The intratubular hyaline casts were commonly observed ($n=13$ out of 21). Intratubular pigments were detected in four patients with COVID-19 (1, 2, 3, and 9). No viral inclusions or nuclear dystrophies were found. Congestion within glomerular and peritubular capillaries (PTC) was respectively observed in 56% and 88% of patients in the COVID-19 group, whereas only one control patient (R2) showed PTC aggregation of erythrocytes. Serial staining for CD61 and CD42b evidenced platelets within the congestive PTC in 11 out of 15 patients (including R2) and within the glomerular capillaries in seven out of nine patients (including R2) (Supplemental Figure 1). Fibrin was not found using Martius Blue Scarlett staining. No proliferative glomerular lesions or modifications of the glomerular basement membrane were observed, except for two patients with COVID-19 (12 and 14) with increased mesangial cellularity. One patient with COVID-19 (8) also showed endocapillary proliferation, with no significant immunoreactive signal for IgA, IgG, IgM, C1q, C4d, and C3. Few patients in the COVID-19 group exhibited endothelial cell swelling in the glomerular capillary loops (11) or the arterioles (4). One patient with COVID-19 (6) showed mild intimal arteritis in only one arterial cross-section. Peritubular capillaritis was observed in three patients with COVID-19 (3, 6, and 8) and the control R1 patient (Figure 1). ACE2 was predominantly located at the brush border of PT cells, and at the surface of the parietal epithelial cells of the glomeruli (Supplemental Figure 2). No ACE2 staining was noticed in the endothelial cells or the distal tubule (DT). No significant difference in the expression and distribution of ACE2 was observed between COVID-19 versus control groups. A significant correlation was found between ATN severity and AKI staging (Spearman correlation = 0.683; $P=0.03$). No other relevant correlation was obtained between the clinical or biologic parameters and histologic findings, especially between the KDIGO stage of proteinuria or the *postmortem* delay of kidney biopsies and PT vacuolization.

## Ultrastructural Findings

The examination of kidney samples by electron microscopy showed clathrin-coated vesicles characterized by an electron-lucent center (approximately 50 nm in diameter) surrounded by an electron-dense capsule (approximately 100 nm in diameter) in three patients (2, 7, and 9) (Figure 2). Typically, these particles face the cell cytoplasm and are inside the plasma membrane, which casts doubt on a viral origin (42). Other ultrastructural features included occasional dense deposits in mesangial or subendothelial locations, and red blood cell congestion in glomerular capillary loops and PTC (Figure 2).

## Detection of SARS-CoV-2 in the Renal Parenchyma Using Immunostaining Against the 2019-nCoV NP, ISH, and Bulk RNA RT-PCR

Immunostaining for the 2019-nCov NP was positive in nine out of 16 patients with COVID-19, as simultaneously confirmed by the specific immunoreactive signal observed in lung sections of guinea pigs infected by SARS-CoV-2. Serial sections with markers of PT (CD10), DT (NCC), and endothelial (CD31) cells revealed a preferential localization of the virus in the cytoplasm of PT cells and in the basolateral pole of the cytoplasm of scattered epithelial cells lining the NCC-positive DT (Figure 3, Supplemental Figures 3 and 4). None of the kidney samples from the control group showed such a dot-shaped signal for the 2019-nCov NP. A faint unspecific immunoreactivity was observed in the cytoplasm of necrotic PT cells in both COVID-19 and control groups. No CD31-positive endothelial cells were positive for the 2019-nCov NP. The extent of tubular positivity for 2019-nCov NP was semiquantitatively scored (on a Banff-derived classification [38]) as <1% in six patients (6, 7, 8, 10, 11, and 14), 1%–10% in two patients (1 and 9), and >10% of all tubules/ducts in one patient (3) (Table 2). Interestingly, the semiquantitative viral load after classic nasopharyngeal sampling had been quantified in five out of 16 patients right before death, with a median delay of 2 (1; 3) days. Two patients (13 and 16) had undetectable levels of SARS-CoV-2, whereas three patients (7, 8, and 10) showed persistent viral load, with a median cycle threshold of 27.12 (20.7–31.6) for the E gene of SARS-CoV-2. The immunostaining against 2019-nCov NP on the corresponding kidney samples was negative in patients with undetectable viral load and positive in patients with measurable viral load. The viremia was not available in our series.

A total of nine out of 16 samples were interpretable by the means of ISH, which contained between three and 10 glomeruli (average of seven glomeruli per specimen). We defined interpretable as being when we could evaluate the presence or the absence of a signal and when positive (housekeeping) and negative controls (bacterial probe) yielded consistent results. In seven patients, there were discrepancies between these three factors that would not allow us to make a clear definition. For this reason, the limitations with tissue availability (no chance to repeat the assays in triplicate, as required) and the potential confounding effect of autopsy material, we decided to report nine samples with high level of certainty and the remaining seven samples as inconclusive. Two samples were positive for nCoV2019-S by ISH: 2 (negative by IHC); 4 (negative by IHC). Two additional samples were considered borderline positive in glomeruli: 11 (negative by IHC) and 9 (negative by IHC). Four samples were considered borderline positive in the tubular-interstitial compartment: 11 (positive by IHC); 9 (positive by IHC); 8 (positive by IHC); and 5 (negative by IHC). The remaining three ISH-negative samples were positive (1 and 10) or negative (15) for the 2019-nCov NP by IHC. All of these findings have been summarized in Table 2. The ISH signal was detected in scattered cells lining the LTL-positive PT and the LTL-negative periglomerular DTs, and in the glomeruli and small vessels (Figure 4, Supplemental Figure 5). Positive and negative controls are provided in Supplemental Figures 6 and 7.

RT-PCR performed from total RNA extracted from FFPE tissue failed to amplify the E and N1/N2 genes of SARS-CoV-2 in kidney samples, except for one patient (15; CT values of and 32.38 for E and N genes, respectively). The median CT value for

**Table 2. Clinical data and most relevant acute renal lesions observed by light microscopy, immunostaining, *in situ* hybridization**

| Patient Status | Glomeruli Tubulointerstitium Peritubular Capillaries Severe Acute Respiratory Syndrome Coronavirus 2 Clinical Data | | | | | | | | | | | | | | | |
|---|---|---|---|---|---|---|---|---|---|---|---|---|---|---|---|---|
| | Patient ID | Ischemia | Capillary Congestion | Endothelial Cell Swelling | Acute Tubular Necrosis | | Tubular vacuolization | Capillaritis | Congestion | IHC | ISH | | DM | HTN | AKI stage | Proteinuria mg/g |
| | | | | | Severity | Extent | | | | Tubules | Glomeruli | Tubules | | | | |
| COVIDICU | 3 | N | Y | N | Mild | >0%–25% | N | ptc1 | Y | >10% | NA | NA | N | Y | 2 | 333 |
| | 4 | Y | Y | N | Mild | >0%–25% | >0%–25% | ptc0 | Y | N | Y | Y | Y | N | N | 595 |
| | 6 | Y | Y | N | Mild | 26%–50% | N | ptc1 | Y | <1% | NA | NA | N | Y | 2 | 453 |
| | 7 | Y | N | N | Severe | >50% | >0%–25%[a,b] | ptc0 | Y | <1% | NA | NA | N | Y | RRT | 353 |
| | 8 | N | N | N | Severe | >50% | N | ptc2 | Y | <1% | N | Bdl | N | N | RRT | 689 |
| | 10 | N | N | N | Severe | >50% | N | ptc0 | Y | <1% | N | N | Y | Y | RRT | 317 |
| | 11 | N | Y | Y | Mild | 26%–50% | 26%–50%[a,b] | ptc0 | Y | <1% | Bdl | Bdl | N | N | 1 | 230 |
| | 13 | N | Y | N | Mild | >0%–25% | >0%–25% | ptc0 | Y | N | NA | NA | Y | Y | 3 | 834 |
| | 15 | N | Y | N | Moderate | >50% | >0%–25% | ptc0 | N | N | N | N | N | Y | 2 | 728 |
| | 16 | N | N | N | Mild | >50% | N | ptc0 | Y | N | NA | NA | Y | N | N | 1484 |
| COVID Non-ICU | 1 | Y | Y | N | Mild | >0%–25% | N | ptc0 | Y | 1%–10% | N | N | Y | N | N | NA |
| | 2 | N | N | N | Mild | >0%–25% | N | ptc0 | Y | N | Y | Y | Y | Y | N | 303 |
| | 5 | N | N | N | Mild | >0%–25% | >0%–25%* | ptc0 | Y | N | N | Bdl | Y | N | N | 1104 |
| | 9 | N | Y | N | Mild | >0%–25% | >0%–25% | ptc0 | Y | 1%–10% | Bdl | Bdl | Y | Y | N | 268 |
| | 12 | Y | N | N | Mild | >0%–25% | 26%–50% | ptc0 | Y | N | NA | NA | Y | Y | 2 | 6004 |
| | 14 | N | Y | N | Mild | 26%–50% | >0%–25% | ptc0 | N | <1% | NA | NA | N | Y | 1 | 579 |
| Control ICU | P1 | N | N | Y | Mild | 26%–50% | N[a] | ptc0 | N | N | | | N | N | 1 | 654 |
| | R1 | Y | N | N | Severe | >50% | >50% | ptc2 | N | N | | | N | Y | 3 | 387 |
| | R2 | N | N | N | Severe | >50% | N[a] | ptc0 | Y | N | | | Y | N | 2 | 2607 |
| | R3 | N | N | N | Moderate | >50% | >0%–25%[a] | ptc0 | N | N | | | Y | Y | RRT | NA |
| | R4 | N | N | N | Severe | >50% | 26%–50% | ptc0 | N | N | | | N | N | 2 | NA |

Capillaritis was scored according to the Banff scoring system (0, <10% cortical PTC containing leukocytes; 1, ≥10% cortical PTC containing 3–4 leukocytes; 2, ≥10% cortical PTC containing 5–10 leukocytes) (41). ID, identification number; IHC, immunohistochemistry; ISH, in situ hybridization; DM, diabetes mellitus; HTN, hypertension; COVID, coronavirus disease; ICU, intensive care unit; N, not detected; Y, detected; NA, not available; PTC, peritubular capillaries; Bdl, borderline.

aPatients exposed to IV contrast.

bPatients treated by calcineurin inhibitor.

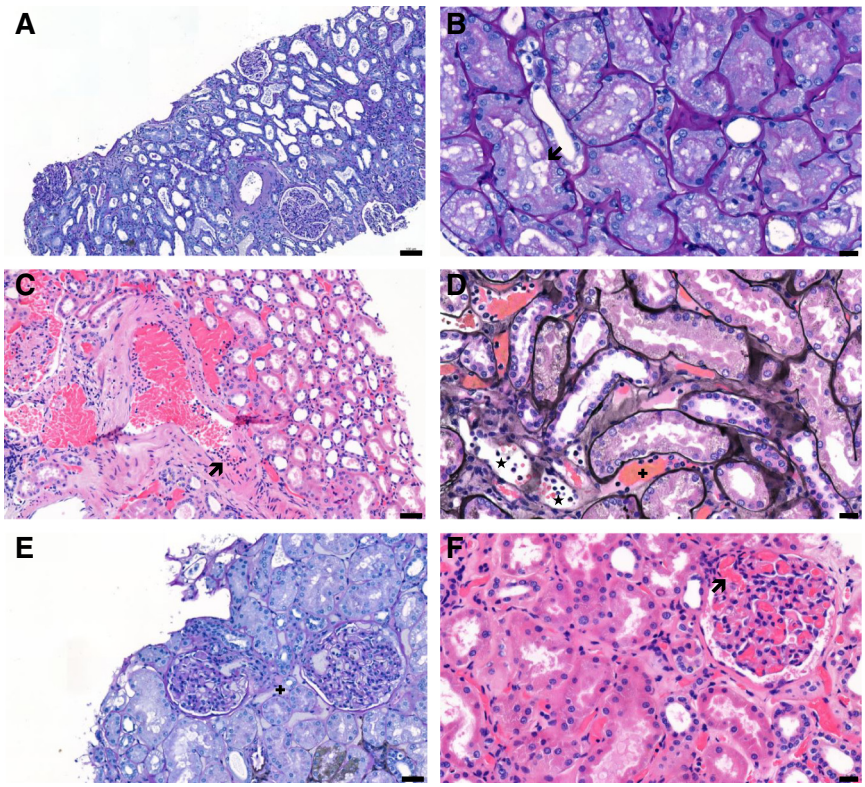


**Figure 1. | Representative histologic findings in *postmortem* kidney biopsies from patients with coronavirus disease 2019 (COVID-19).** (A) Acute tubular necrosis with thinning of the tubular epithelium, loss of brush border, and cell shedding (Periodic Acid Shiff [PAS] staining, patient 7); (B) cytoplasmic vacuolization (arrow) of proximal tubular epithelial cells (PAS staining, patient 14); (C) intimal arteritis (arrow; hematoxylin and eosin staining, patient 6); (D) peritubular capillaritis (*) and congestion in peritubular capillaries (+); Jones staining, patient 3; (E) glomerular endothelial cell swelling and congestion in peritubular capillaries (+; PAS staining, patient 11); and (F) congestion in glomerular capillaries (arrow; PAS staining, patient 6). Scale bars = 100 μm (A), 20 μm (B, D, and F), 50 μm (C and E).

human RNAseP gene reached 20.89 (18.39; 26.27) in the whole cohort.

## Discussion

COVID-19 is a novel nosological entity, with a broad clinical spectrum. The early description of the entity logically focused on lung involvement, although an increasing number of reports have progressively highlighted the effect of SARS-CoV-2 on other organs, including the kidneys (3,6–8). Furthermore, correlations between extrarespiratory viral tropism, disease severity, and increased risk of premature death within the first 3 weeks of disease have been highlighted (7). In our prospective cohort on the basis of immediate *postmortem* kidney biopsies, we observed ATN in all patients, with unusual congestion of the glomerular and PTC. No thrombi were factually evidenced. No tubulitis or interstitial inflammation was found. No viral inclusions or nuclear dystrophies were observed. Although SARS-CoV-2 genes could not be consistently detected by the means of RT-PCR of bulk RNA from FFPE kidney samples, a positive signal for SARS-CoV-2 was found at both protein and RNA levels, with a preferential localization in the cytoplasm of both PT and DT cells. SARS-CoV-2 mRNA was also detected in a few glomerular and endothelial cells.

Our findings strengthen the first histologic observations highlighting a preferentially tubular pattern of kidney injury, including ATN lesions and PT vacuolization (25). Of important note, endothelial lesions, such as cell swelling with foamy degeneration and subendothelial expansion and proliferation, had been described in this initial report (25). The hypoxic delay between death and renal sampling may partly explain this pattern of endothelium injury. Examination by electron microscopy showed clusters of particles with distinctive spikes in podocytes and epithelial cells lining the renal tubules. However, these aspects of "virus-like particles" have been strongly challenged because they may correspond to physiologic intracellular components such as clathrin-coated vesicles and multivesicular bodies, as observed in our cohort (26,42,43). Note that the timing and the location of the kidney biopsy, and the expertise of the observer(s), may also influence the yield of electromicroscopy-based identification of viral particles. The nucleoprotein of SARS-CoV-2 was then found in unspecified renal tubules (44). Another *postmortem* case series (with a mean hypoxic delay of 33 hours) demonstrated diffuse ATN, with three out of 18 patients showing fibrin thrombi in glomerular capillaries (45). Thrombosis of the renal microvasculature has also been highlighted in *postmortem* kidney samples from patients who benefited from extended cardiopulmonary resuscitation (CPR) before death (27). CPR-associated ischemia may significantly affect the renal microvasculature. In our cohort, all patients died from septic shock or ARDS, with no prior CPR. In total, 75% of our patients were on anticoagulation therapy during their stay. No thrombotic

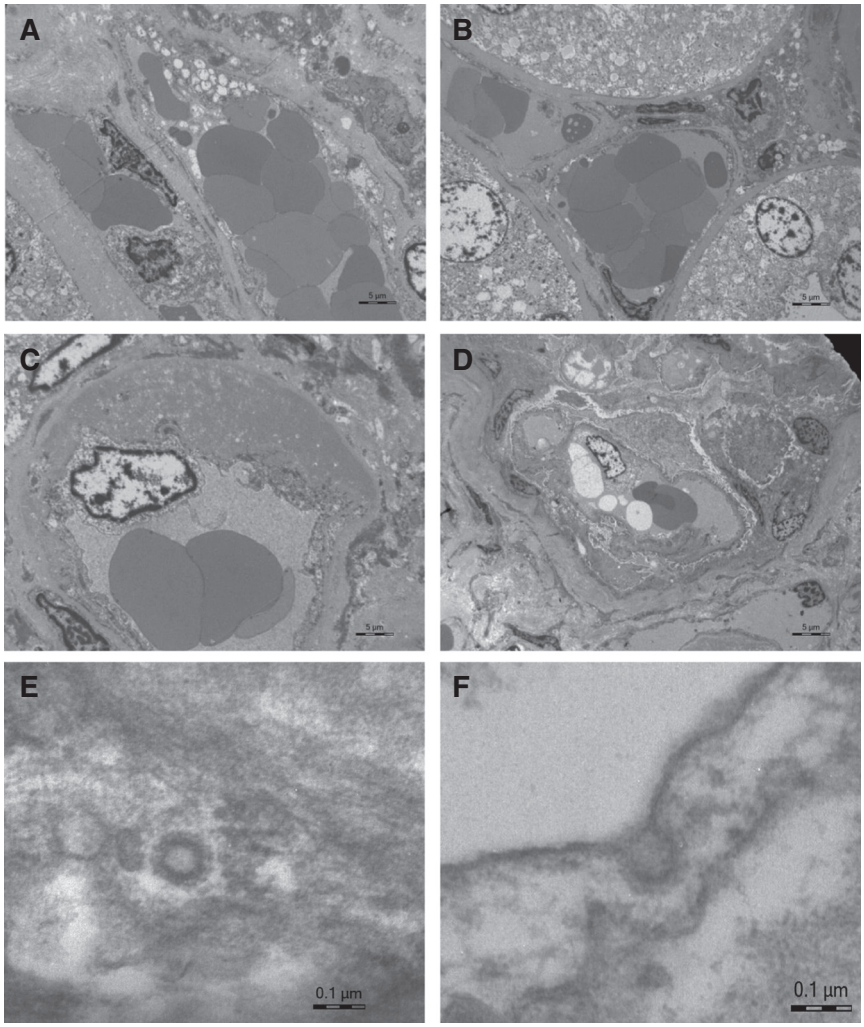


**Figure 2.** | **Ultrastructural findings in *postmortem* kidney biopsies from patients with coronavirus disease 2019 (COVID-19).** (A–C) Congestion of red blood cells in peritubular capillaries and expansion of subendothelial space (C) by accumulation of an amorphous osmiophilic material; (patient 5). (D) Congestion in a glomerular capillary loop (patient 4); (E and F) Viral-like particles corresponding to clathrin-coated vesicles in a glomerular capillary loop (E) and in a renal cortical artery (F) (patient 2). Scale bars = 5 µm (A–D), 0.1 µm (E and F).

microangiopathy or thrombi within the glomerular capillaries were observed or stained by Martius Blue Scarlett.

Evidence of nephrotic-range proteinuria and collapsing glomerulopathy was reported in patients with COVID-19 (28,46). Diffuse tubulo-reticular inclusions called "IFN footprints" were described in glomerular endothelial cells, which may reflect SARS-CoV-2–induced excessive production of IFN (47). A case series of 10 patients with COVID-19 and AKI, proteinuria, and/or hematuria showed two patients with thrombotic microangiopathy, and one patient with focal sclerosis and features of healing collapsing glomerulopathy in isolated glomeruli. One patient had pauci-immune crescentic GN. All biopsies were negative for the SARS-CoV-2 NP antigen (48). A case series of 17 patients (including three kidney transplant recipients) showed various levels of ATN, with no evidence of SARS-CoV-2 (S2 subunit) in the renal parenchyma (36). Conversely, the spike protein of SARS-CoV-2 was detected in two out of 14 patients with COVID-19, as a patchy, granular cytoplasmic staining in tubular epithelial cells (49). ISH for SARS-CoV-2 was negative in a recent *postmortem* kidney sample study (50). Golmai *et al.* mainly focused on patients with stage 2 or 3 AKI, with high rate of patient requiring RRT ($n=8$ out of 12), whereas patients with and without AKI were eligible in our study. Note that the delay between death and biopsy in Golmai's report ranges between 1.5 and 70 hours, which may increase the risk of autolysis and biased interpretation of the histologic lesions and subsequent technical investigations. Finally, a cohort of 42 autopsies (including six patients deceased before hospital admission) reported on ATN and focal (<5% of glomeruli) fibrin thrombi ($n=6$ patients). Immunostaining against the spike antigen and ISH for SARS-CoV-2 were negative ($n=10$ patients) (51). It is important to remember that all of these tissue-based studies necessarily represent a "snapshot" of a highly dynamic pathologic process, which may explain the heterogeneous findings regarding the presence of SARS-CoV-2 mRNA and/or protein in the renal parenchyma (44). Furthermore, the yield of each technique may be affected by the type of starting materials, such as fresh versus snap frozen, versus FFPE versus RNA later-preserved samples collected *ante* versus *postmortem*.

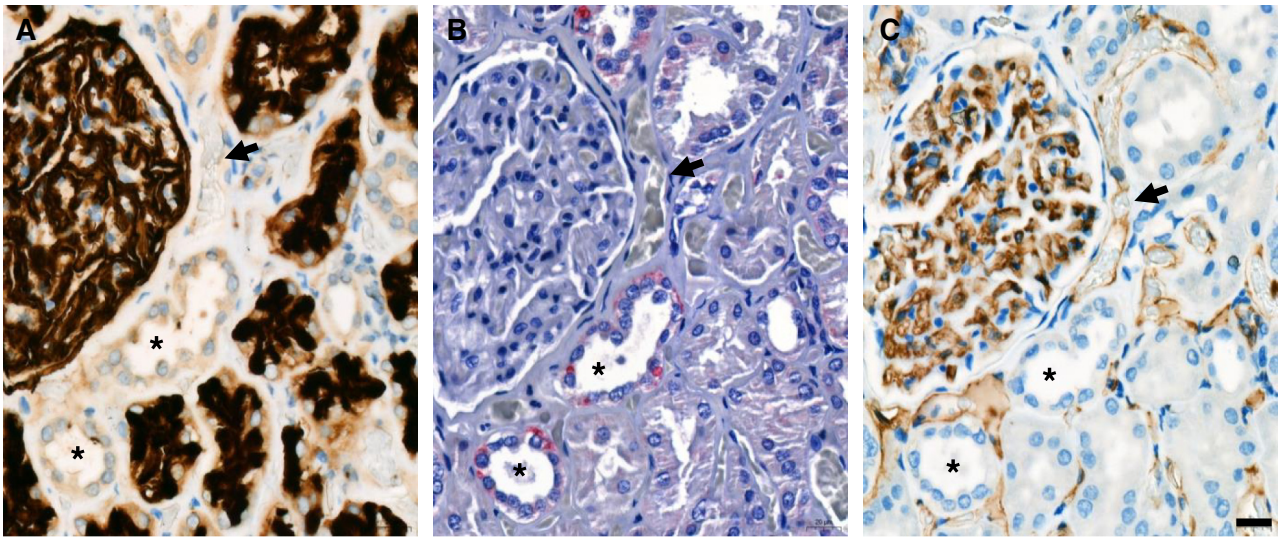


**Figure 3. | Representative serial immunostaining for CD10, 2019-nCov N-Protein, and CD31 on *postmortem* kidney biopsies from a patient with coronavirus disease 2019 (COVID-19).** Serial sections of kidney samples from patients with COVID-19 were used for immunostaining against the proximal tubule marker, CD10 (in black) (A); the 2019-nCov N-Protein (in red) (B); and the endothelial marker, CD31 (in brown) (C). A punctuate pattern for the 2019-nCov N-Protein is detected at the basolateral pole of CD10-negative and CD31-negative distal tubule (*) (patient 9). No specific signal is detected in CD31-positive peritubular capillaries (arrow). Scale bars = 20 μm

The limitations of our monocentric study include the small number of observations, which prevents us from building robust correlation between the clinical parameters and the histologic findings. We have no information about the viremia in our cohort. Of note, positive SARS-CoV-2 viremia has been reported as detectable in <40% of patients with COVID-19 pneumonia (52,53). We provide a detailed clinical and biologic description of all patients, thereby allowing correlations and comparisons to previous reports (summarized in Supplemental Table 4). As a reminder, patients with or without AKI were eligible in our study, which allowed us to cover an extended spectrum of the COVID-19–associated nephropathy. The *postmortem* collection of the renal samples may bias the specific identification of renal COVID-19–associated lesions because the features of ATN and *postmortem* autolysis are very similar. To circumvent this limitation, we have included five archival kidney samples from patients with septic shock and/or ARDS, and we collected most of the samples within 1 hour after death. Note that four out of five control tissue specimens were extracted from a historical pathology bank and did not *stricto sensu* follow the same path of harvesting and processing of the COVID-19 tissue samples. All biopsies were methodically described by three experienced renal pathologists following *a priori* well-standardized criteria, to limit the interobserver variability in the description and scoring of the morphologic features. The severity of the ATN was not different between COVID-19 versus control groups. No immune deposits or interstitial inflammation were found in our series. Conversely, the nonthrombotic congestion in glomerular and peritubular capillaries was preferentially observed in patients with COVID-19. Due to the small sample size of the control group, COVID-19–associated capillary congestion must be interpreted with caution. Still, peritubular capillary congestion has been described in other clinical entities, including hantavirus infection (probably secondary to increased endothelial permeability [54]) and renal ischemia/reperfusion (55). A sepsis-induced decreased of renal perfusion in patients with COVID-19 may also contribute to this histopathological observation. Of important note against the hypothesis of nonspecific random morphologic *postmortem* observation, the capillary congestion is not considered a major criterion of ATN caused by autolysis (56). Our observations, based both on *ISH* and immunostaining, support a SARS-CoV-2 kidney tropism in both proximal and DTs, despite the absence of definitive ultrastructural evidence. The significance of one single patient with positive RT-PCR characterized by a high CT number is questionable. Still, the negative and positive controls of this experiment performed on total RNA extracted from FFPE tissue were repeatedly concordant with the detection of SARS-CoV-2 E and N genes in the renal bulk RNA of this patient.

In conclusion, our collection of immediate *postmortem* kidney biopsies highlights a congestive pattern of COVID-19–associated AKI, with SARS-CoV-2 detection in different renal compartments, including proximal and distal tubules, glomeruli, and vessels.

## Disclosures

F. Jouret reports having consultancy agreements with ORGENESIS; reports receiving honoraria from AMGEN and OTSUKA; and reports being a scientific advisor or member of the Belgian Society of Nephrology. J.-M. Krzesinski reports having consultancy agreements with Bayer, Boehringer, Menarini, and Vifor Pharma; and reports receiving honoraria from Bayer, Boehringer, Menarini, and Vifor. P. Delanaye reports having consultancy agreements with ARK Biosciences and Immunodiagnostic Systems; and reports receiving honoraria from Amgen, AstraZeneca, Bayer, Fresenius, Menarini, Sanofi, and Siemens. T. Huber reports having consultancy agreements with AstraZeneca, Bayer, Boehringer-Ingelheim, DaVita, Deerfield, Fresenius Medical Care, GoldfinchBio, Mantrabio, Novartis, and Retrophin; reports receiving research funding from Amicus Therapeutics and Fresenius Medical Care; and reports being a scientific advisor or member of Kidney International (Journal; Editorial board) and Nature Review Nephrology (Journal, Advisory Board). All remaining authors have nothing to disclose.

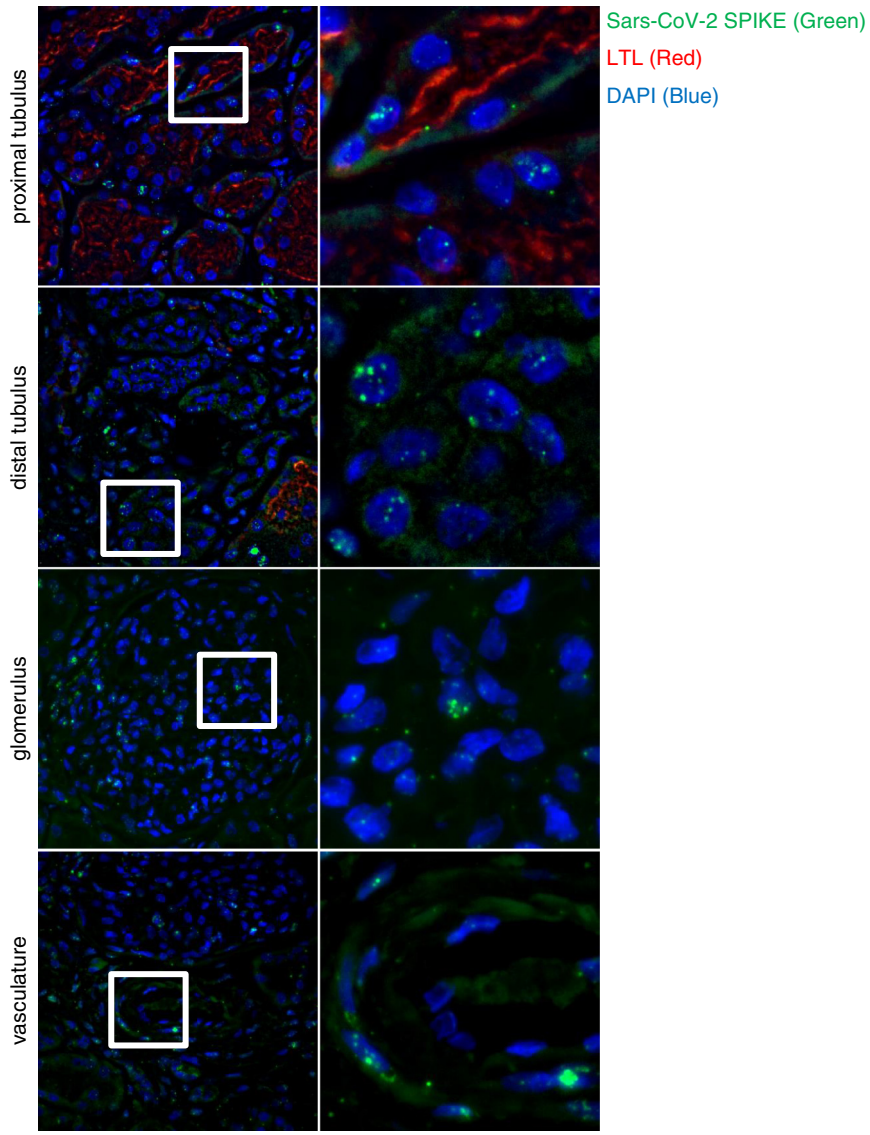


**Figure 4.** | **Detection and spatial distribution of viral RNA using fluorescence *in situ* hybridization.** The first (overview) and second (targeted zoom) columns display positive signal for viral RNA in different renal compartments, including proximal and distal tubules, glomeruli, and vessels. nCoV2019-S RNA is in green; *Lotus tetragonolobus* lectin (LTL) is in red; DAPI is in blue (patient 4).


## Funding

This work is supported by the ULiège Fondation Léon Frédéricq and Fonds National de la Recherche Scientifique. T.B. Huber and V.G. Puelles were supported by the German Research Foundation (DFG) grant CRC1192 and the Federal Ministry of Education and Research (BMBF) DEFEAT PANDEMIcs autopsy network. T.B. Huber was additionally supported by the DFG grants HU 1016/8-2, HU 1016/11-1, and HU 1016/12-1, and by the BMBF grant STOP-FSGS-01GM1901C. V.G. Puelles was also supported by the BMBF eMed Consortia Fibromap.

## Acknowledgments

The authors sincerely thank all physicians and nurses who take care of patients with COVID-19 in the clinical wards and ICUs. The authors also thank all members of the department of Medico-Economic Information Service, Laurence Poma (ULiège Cardiovascular Sciences), François Maclot (ULiège Academic Hospital, Department of Clinical Microbiology), and Michael Sarlet (ULiège, School of Veterinary Medicine) for their technical assistance. Our manuscript has been reviewed by a native English speaker, Enda Breen (enda.breen4@mail.dcu.ie), who is a member of the Irish Translators' and Interpreters' Association. P. Erpicum, J. Huart, and F. Jouret are Fellows of the Fonds National de la Recherche Scientifique, Brussels, Belgium.


## Author Contributions

A. Bouquegneau, P. Delanaye, P. Delvenne, F. Jouret, J.-M. Krzesinski, and B. Misset conceptualized the study; A. Bouquegneau, P. Erpicum, and S. Grosch were responsible for the data curation; A. Bouquegneau, C. Bovy, P. Delanaye, P. Erpicum, F. Jouret, L. Habran, M.-P. Hayette, O. Hougrand, J. Huart, T. B. Huber, D. Kylies, and V. G. Puelles were responsible for the formal analysis; A. Bouquegneau and P. Erpicum were responsible for the investigation; A. Bouquegneau, C. Bovy, P. Delanaye, P. Erpicum, S. Grosch, L. Habran, O. Hougrand, F. Jouret, D. Kylies, and V. G. Puelles were responsible for the methodology; A. Bouquegneau, C. Bovy, P. Delanaye, P. Delvenne, P. Erpicum, S. Grosch, J. Huart, M.-P. Hayette, F. Jouret, and V. G. Puelles were responsible for the validation; P. Delanaye and F. Jouret provided supervision; A. Bouquegneau and P. Delanaye were responsible for the visualization; A. Bouquegneau, P.

Delanaye, P. Erpicum, and F. Jouret wrote the original draft; and all authors reviewed, edited, and approved the final version of the manuscript.

## Supplemental Material

This article contains the following supplemental material online at http://kidney360.asnjournals.org/lookup/suppl/doi:10.34067/KID.0006992020/-/DCSupplemental.

Supplemental Table 1. Criteria for the scoring of kidney samples using light microscopy.

Supplemental Table 2. Clinical and biological characteristics of the patients infected with SARS-CoV-2 by type of hospitalization ward.

Supplemental Table 3. Clinical and biological characteristics of the control group (patients who are not SARS-CoV-2 infected).

Supplemental Table 4. Summary of the case series using kidney biopsies of patients infected with SARS- CoV-2.

Supplemental Figure 1. Nonthrombotic congestion in glomerular and peritubular capillaries of kidney samples from patients with COVID-19.

Supplemental Figure 2. Representative immunostaining for angiotensin-converting enzyme 2 (ACE2) in postmortem paraffin-embedded kidney tissue from a patient with COVID-19 (patient 11).

Supplemental Figure 3. Representative immunostaining for SARS-CoV-2 nucleocapsid protein at low magnification in postmortem paraffin-embedded kidney tissue from patients with COVID-19 (patients 1 and 3).

Supplemental Figure 4. Immunostaining for (A) nucleocapsid N protein of the SARS-CoV-2 (NP) and (B) sodium-chloride cotransporter (NCC) on serial paraffin-embedded sections (patient 6).

Supplemental Figure 5. Detection and spatial distribution of viral RNA using fluorescence in situ hybridization.

Supplemental Figure 6. Experimental controls of the fluorescent in situ hybridization experiment.

Supplemental Figure 7. Experimental controls of the immunostaining experiment.

## References


1. Zhu N, Zhang D, Wang W, Li X, Yang B, Song J, Zhao X, Huang B, Shi W, Lu R, Niu P, Zhan F, Ma X, Wang D, Xu W, Wu G, Gao GF, Tan W; China Novel Coronavirus Investigating and Research Team: A novel coronavirus from patients with pneumonia in China, 2019. N Engl J Med 382: 727–733, 2020 https://doi.org/10.1056/NEJMoa2001017
2. Li Q, Guan X, Wu P, Wang X, Zhou L, Tong Y, Ren R, Leung KSM, Lau EHY, Wong JY, Xing X, Xiang N, Wu Y, Li C, Chen Q, Li D, Liu T, Zhao J, Liu M, Tu W, Chen C, Jin L, Yang R, Wang Q, Zhou S, Wang R, Liu H, Luo Y, Liu Y, Shao G, Li H, Tao Z, Yang Y, Deng Z, Liu B, Ma Z, Zhang Y, Shi G, Lam TTY, Wu JT, Gao GF, Cowling BJ, Yang B, Leung GM, Feng Z: Early transmission dynamics in Wuhan, China, of novel coronavirus-infected pneumonia. N Engl J Med 382: 1199–1207, 2020 https://doi.org/10.1056/NEJMoa2001316
3. Huang C, Wang Y, Li X, Ren L, Zhao J, Hu Y, Zhang L, Fan G, Xu J, Gu X, Cheng Z, Yu T, Xia J, Wei Y, Wu W, Xie X, Yin W, Li H, Liu M, Xiao Y, Gao H, Guo L, Xie J, Wang G, Jiang R, Gao Z, Jin Q, Wang J, Cao B: Clinical features of patients infected with 2019 novel coronavirus in Wuhan, China. Lancet 395: 497–506, 2020 https://doi.org/10.1016/S0140-6736(20)30183-5
4. Guan W-J, Ni Z-Y, Hu Y, Liang W-H, Ou C-Q, He J-X, Liu L, Shan H, Lei C-L, Hui DSC, Du B, Li L-J, Zeng G, Yuen K-Y, Chen R-C, Tang C-L, Wang T, Chen P-Y, Xiang J, Li S-Y, Wang J-L, Liang Z-J, Peng Y-X, Wei L, Liu Y, Hu Y-H, Peng P, Wang J-M, Liu J-Y, Chen Z, Li G, Zheng Z-J, Qiu S-Q, Luo J, Ye C-J, Zhu S-Y, Zhong N-S; China Medical Treatment Expert Group for Covid-19: Clinical characteristics of coronavirus disease 2019 in China. N Engl J Med 382: 1708–1720, 2020 https://doi.org/10.1056/NEJMoa2002032
5. Cheng Y, Luo R, Wang K, Zhang M, Wang Z, Dong L, Li J, Yao Y, Ge S, Xu G: Kidney disease is associated with in-hospital death of patients with COVID-19. Kidney Int 97: 829–838, 2020 https://doi.org/10.1016/j.kint.2020.03.005
6. Puelles VG, Lütgehetmann M, Lindenmeyer MT, Sperhake JP, Wong MN, Allweiss L, Chilla S, Heinemann A, Wanner N, Liu S, Braun F, Lu S, Pfefferle S, Schröder AS, Edler C, Gross O, Glatzel M, Wichmann D, Wiech T, Kluge S, Pueschel K, Aepfelbacher M, Huber TB: Multiorgan and renal tropism of SARS-CoV-2. N Engl J Med 383: 590–592, 2020 https://doi.org/10.1056/NEJMc2011400
7. Braun F, Lütgehetmann M, Pfefferle S, Wong MN, Carsten A, Lindenmeyer MT, Nörz D, Heinrich F, Meißner K, Wichmann D, Kluge S, Gross O, Pueschel K, Schröder AS, Edler C, Aepfelbacher M, Puelles VG, Huber TB: SARS-CoV-2 renal tropism associates with acute kidney injury. Lancet 396: 597–598, 2020 https://doi.org/10.1016/S0140-6736(20)31759-1
8. Huart J, Bouquegneau A, Lutteri L, Erpicum P, Grosch S, Résimont G, Wiesen P, Bovy C, Krzesinski J-M, Thys M, Lambermont B, Misset B, Pottel H, Mariat C, Cavalier E, Burtey S, Jouret F, Delanaye P: Proteinuria in COVID-19: prevalence, characterization and prognostic role. J Nephrol 1–10, 2021 33484426
9. Wang W, Xu Y, Gao R, Lu R, Han K, Wu G, Tan W: Detection of SARS-CoV-2 in different types of clinical specimens. JAMA 323: 1843–1844, 2020 https://doi.org/10.1001/jama.2020.3786
10. Hirsch JS, Ng JH, Ross DW, Sharma P, Shah HH, Barnett RL, Hazzan AD, Fishbane S, Jhaveri KD; Northwell COVID-19 Research Consortium; Northwell Nephrology COVID-19 Research Consortium: Acute kidney injury in patients hospitalized with COVID-19. Kidney Int 98: 209–218, 2020 https://doi.org/10.1016/j.kint.2020.05.006
11. Ng JH, Hirsch JS, Hazzan A, Wanchoo R, Shah HH, Malieckal DA, Ross DW, Sharma P, Sakhiya V, Fishbane S, Jhaveri KD; Northwell Nephrology COVID-19 Research Consortium: Outcomes among patients hospitalized with COVID-19 and acute kidney injury. Am. J. Kidney Dis 77: 204–215.e1, 2021
12. Pedersen SF, Ho Y-C: SARS-CoV-2: A storm is raging. J Clin Invest 130: 2202–2205, 2020 https://doi.org/10.1172/JCI137647
13. Mehta P, McAuley DF, Brown M, Sanchez E, Tattersall RS, Manson JJ; HLH Across Speciality Collaboration, UK: COVID-19: Consider cytokine storm syndromes and immunosuppression. Lancet 395: 1033–1034, 2020 https://doi.org/10.1016/S0140-6736(20)30628-0
14. Tang N, Li D, Wang X, Sun Z: Abnormal coagulation parameters are associated with poor prognosis in patients with novel coronavirus pneumonia. J Thromb Haemost 18: 844–847, 2020 https://doi.org/10.1111/jth.14768
15. Zhang Y, Xiao M, Zhang S, Xia P, Cao W, Jiang W, Chen H, Ding X, Zhao H, Zhang H, Wang C, Zhao J, Sun X, Tian R, Wu W, Wu D, Ma J, Chen Y, Zhang D, Xie J, Yan X, Zhou X, Liu Z, Wang J, Du B, Qin Y, Gao P, Qin X, Xu Y, Zhang W, Li T, Zhang F, Zhao Y, Li Y, Zhang S: Coagulopathy and antiphospholipid antibodies in patients with covid-19. N Engl J Med 382: e38, 2020 https://doi.org/10.1056/NEJMc2007575
16. Hamming I, Timens W, Bulthuis MLC, Lely AT, Navis G, van Goor H: Tissue distribution of ACE2 protein, the functional receptor for SARS coronavirus. A first step in understanding SARS pathogenesis. J Pathol 203: 631–637, 2004 https://doi.org/10.1002/path.1570
17. Ye M, Wysocki J, William J, Soler MJ, Cokic I, Batlle D: Glomerular localization and expression of Angiotensin-converting enzyme 2 and Angiotensin-converting enzyme: Implications for albuminuria in diabetes. J Am Soc Nephrol 17: 3067–3075, 2006 https://doi.org/10.1681/ASN.2006050423
18. Kormann R, Jacquot A, Alla A, Corbel A, Koszutski M, Voirin P, Garcia Parrilla M, Bevilacqua S, Schvoerer E, Gueant J-L, Namour F, Levy B, Frimat L, Oussalah A: Coronavirus disease 2019: Acute Fanconi syndrome precedes acute kidney injury. Clin Kidney J 13: 362–370, 2020 https://doi.org/10.1093/ckj/sfaa109
19. Aguiar JA, Tremblay BJ-M, Mansfield MJ, Woody O, Lobb B, Banerjee A, Chandiramohan A, Tiessen N, Cao Q, Dvorkin-Gheva A, Revill S, Miller MS, Carlsten C, Organ L, Joseph C, John A, Hanson P, Austin RC, McManus BM, Jenkins G, Mossman K, Ask K, Doxey AC, Hirota JA: Gene expression and *in situ* protein profiling of candidate SARS-CoV-2 receptors in

human airway epithelial cells and lung tissue. Eur Respir J 56: 2001123, 2020 https://doi.org/10.1183/13993003.01123-2020
20. Su H, Wan C, Wang Z-D, Gao Y, Li Y-C, Tang F, Zhu H-Y, Yi L-X, Zhang C: Expression of CD147 and cyclophilin A in kidneys of patients with COVID-19. Clin J Am Soc Nephrol 16: 618–619, 2021
21. Lely AT, Hamming I, van Goor H, Navis GJ: Renal ACE2 expression in human kidney disease. J Pathol 204: 587–593, 2004 https://doi.org/10.1002/path.1670
22. Soler MJ, Ye M, Wysocki J, William J, Lloveras J, Batlle D: Localization of ACE2 in the renal vasculature: Amplification by angiotensin II type 1 receptor blockade using telmisartan. Am J Physiol Renal Physiol 296: F398–F405, 2009 https://doi.org/10.1152/ajprenal.90488.2008
23. Peng L, Liu J, Xu W, Luo Q, Chen D, Lei Z, Huang Z, Li X, Deng K, Lin B, Gao Z: SARS-CoV-2 can be detected in urine, blood, anal swabs, and oropharyngeal swabs specimens. J Med Virol 92: 1676–1680, 2020 https://doi.org/10.1002/jmv.25936
24. Wölfel R, Corman VM, Guggemos W, Seilmaier M, Zange S, Müller MA, Niemeyer D, Jones TC, Vollmar P, Rothe C, Hoelscher M, Bleicker T, Brünink S, Schneider J, Ehmann R, Zwirglmaier K, Drosten C, Wendtner C: Virological assessment of hospitalized patients with COVID-2019 [published correction appears in Nature 588: E35, 2020 10.1038/s41586-020-2984-3]. Nature 581: 465–469, 2020 https://doi.org/10.1038/s41586-020-2196-x
25. Su H, Yang M, Wan C, Yi L-X, Tang F, Zhu H-Y, Yi F, Yang H-C, Fogo AB, Nie X, Zhang C: Renal histopathological analysis of 26 postmortem findings of patients with COVID-19 in China. Kidney Int 98: 219–227, 2020 https://doi.org/10.1016/j.kint.2020.04.003
26. Farkash EA, Wilson AM, Jentzen JM: Ultrastructural evidence for direct renal infection with SARS-CoV-2. J Am Soc Nephrol 31: 1683–1687, 2020 https://doi.org/10.1681/ASN.2020040432
27. Rapkiewicz AV, Mai X, Carsons SE, Pittaluga S, Kleiner DE, Berger JS, Thomas S, Adler NM, Charytan DM, Gasmi B, Hochman JS, Reynolds HR: Megakaryocytes and platelet-fibrin thrombi characterize multi-organ thrombosis at autopsy in COVID-19: A case series. EClinicalMedicine 24: 100434, 2020 https://doi.org/10.1016/j.eclinm.2020.100434
28. Wu H, Larsen CP, Hernandez-Arroyo CF, Mohamed MMB, Caza T, Sharshir M, Chughtai A, Xie L, Gimenez JM, Sandow TA, Lusco MA, Yang H, Acheampong E, Rosales IA, Colvin RB, Fogo AB, Velez JCQ: AKI and collapsing glomerulopathy associated with COVID-19 and *APOL1* high-risk genotype. J Am Soc Nephrol 31: 1688–1695, 2020 https://doi.org/10.1681/ASN.2020050558
29. Wichmann D, Sperhake J-P, Lütgehetmann M, Steurer S, Edler C, Heinemann A, Heinrich F, Mushumba H, Kniep I, Schröder AS, Burdelski C, de Heer G, Nierhaus A, Frings D, Pfefferle S, Becker H, Bredereke-Wiedling H, de Weerth A, Paschen H-R, Sheikhzadeh-Eggers S, Stang A, Schmiedel S, Bokemeyer C, Addo MM, Aepfelbacher M, Püschel K, Kluge S: Autopsy findings and venous thromboembolism in patients with COVID-19: A prospective cohort study. Ann Intern Med 173: 268–277, 2020 https://doi.org/10.7326/M20-2003
30. Corman VM, Landt O, Kaiser M, Molenkamp R, Meijer A, Chu DK, Bleicker T, Brünink S, Schneider J, Schmidt ML, Mulders DG, Haagmans BL, van der Veer B, van den Brink S, Wijsman L, Goderski G, Romette J-L, Ellis J, Zambon M, Peiris M, Goossens H, Reusken C, Koopmans MP, Drosten C: Detection of 2019 novel coronavirus (2019-nCoV) by real-time RT-PCR [published correction appears in Euro Surveill 25: 2007303, 2020 10.2807/1560-7917.ES.2020.25.30.2007303]. Euro Surveill 25: 2000045, 2020 https://doi.org/10.2807/1560-7917.ES.2020.25.3.2000045
31. Artesi M, Bontems S, Göbbels P, Franckh M, Maes P, Boreux R, Meex C, Melin P, Hayette M-P, Bours V, Durkin K: A recurrent mutation at position 26340 of SARS-CoV-2 is associated with failure of the E gene quantitative reverse transcription-PCR utilized in a commercial dual-target diagnostic assay. J Clin Microbiol 58: e01598–e20, 2020 https://doi.org/10.1128/JCM.01598-20
32. Matsushita K, Mahmoodi BK, Woodward M, Emberson JR, Jafar TH, Jee SH, Polkinghorne KR, Shankar A, Smith DH, Tonelli M, Warnock DG, Wen C-P, Coresh J, Gansevoort RT, Hemmelgarn BR, Levey AS; Chronic Kidney Disease Prognosis Consortium: Comparison of risk prediction using the CKD-EPI equation and the MDRD study equation for estimated glomerular filtration rate. JAMA 307: 1941–1951, 2012 https://doi.org/10.1001/jama.2012.3954
33. Stevens Paul E, Levin Adeera; Kidney Disease: Improving Global Outcomes Chronic Kidney Disease Guideline Development Work Group Members: Evaluation and management of chronic kidney disease: synopsis of the kidney disease: improving global outcomes 2012 clinical practice guideline. Ann Intern Med 158[11]: 825–830, 2013 10.7326/0003-4819-158-11-201306040-00007 23732715
34. Kellum JA, Lameire N; KDIGO AKI Guideline Work Group: Diagnosis, evaluation, and management of acute kidney injury: A KDIGO summary (Part 1). Crit Care 17: 204, 2013 https://doi.org/10.1186/cc11454
35. Chung M, Bernheim A, Mei X, Zhang N, Huang M, Zeng X, Cui J, Xu W, Yang Y, Fayad ZA, Jacobi A, Li K, Li S, Shan H: CT imaging features of 2019 novel coronavirus (2019-nCoV). Radiology 295: 202–207, 2020 https://doi.org/10.1148/radiol.2020200230
36. Kudose S, Hoshi M, Jain S, Gaut JP: Renal histopathologic findings associated with severity of clinical acute kidney injury. Am J Surg Pathol 42: 625–635, 2018 https://doi.org/10.1097/PAS.0000000000001028
37. Liu J, Babka AM, Kearney BJ, Radoshitzky SR, Kuhn JH, Zeng X: Molecular detection of SARS-CoV-2 in formalin-fixed, paraffin-embedded specimens. JCI Insight 5: e139042, 2020 https://doi.org/10.1172/jci.insight.139042
38. Nickeleit V, Singh HK, Randhawa P, Drachenberg CB, Bhatnagar R, Bracamonte E, Chang A, Chon WJ, Dadhania D, Davis VG, Hopfer H, Mihatsch MJ, Papadimitriou JC, Schaub S, Stokes MB, Tungekar MF, Seshan SV; Banff Working Group on Polyomavirus Nephropathy: The Banff working group classification of definitive polyomavirus nephropathy: Morphologic definitions and clinical correlations. J Am Soc Nephrol 29: 680–693, 2018 https://doi.org/10.1681/ASN.2017050477
39. Bonin S, Hlubek F, Benhattar J, Denkert C, Dietel M, Fernandez PL, Höfler G, Kothmaier H, Kruslin B, Mazzanti CM, Perren A, Popper H, Scarpa A, Soares P, Stanta G, Groenen PJTA: Multicentre validation study of nucleic acids extraction from FFPE tissues. Virchows Arch 457: 309–317, 2010 https://doi.org/10.1007/s00428-010-0917-5
40. Wang F, Flanagan J, Su N, Wang L-C, Bui S, Nielson A, Wu X, Vo H-T, Ma X-J, Luo Y: RNAscope: A novel *in situ* RNA analysis platform for formalin-fixed, paraffin-embedded tissues. J Mol Diagn 14: 22–29, 2012 https://doi.org/10.1016/j.jmoldx.2011.08.002
41. Roufosse C, Simmonds N, Clahsen-van Groningen M, Haas M, Henriksen KJ, Horsfield C, Loupy A, Mengel M, Perkowska-Ptasińska A, Rabant M, Racusen LC, Solez K, Becker JU: A 2018 reference guide to the Banff classification of renal allograft pathology. Transplantation 102: 1795–1814, 2018 https://doi.org/10.1097/TP.0000000000002366
42. Miller SE, Brealey JK: Visualization of putative coronavirus in kidney. Kidney Int 98: 231–232, 2020 https://doi.org/10.1016/j.kint.2020.05.004
43. Frelih M, Erman A, Wechtersbach K, Pleško J, Avšič-Županc T, Kojc N: SARS-CoV-2 virions or ubiquitous cell structures? Actual dilemma in COVID-19 era. Kidney Int Rep 5: 1608–1610, 2020 https://doi.org/10.1016/j.ekir.2020.07.003
44. Müller JA, Groß R, Conzelmann C, Krüger J, Merle U, Steinhart J, Weil T, Koepke L, Bozzo CP, Read C, Fois G, Eiseler T, Gehrmann J, van Vuuren J, Wessbecher IM, Frick M, Costa IG, Breunig M, Grüner B, Peters L, Schuster M, Liebau S, Seufferlein T, Stenger S, Stenzinger A, MacDonald PE, Kirchhoff F, Sparrer KMJ, Walther P, Lickert H, Barth TFE, Wagner M, Münch J, Heller S, Kleger A: SARS-CoV-2 infects and replicates in cells of the human endocrine and exocrine pancreas. Nat Metab 3: 149–165, 2021 33536639
45. Menter T, Haslbauer JD, Nienhold R, Savic S, Hopfer H, Deigendesch N, Frank S, Turek D, Willi N, Pargger H, Bassetti S,

Leuppi JD, Cathomas G, Tolnay M, Mertz KD, Tzankov A: Postmortem examination of COVID-19 patients reveals diffuse alveolar damage with severe capillary congestion and variegated findings in lungs and other organs suggesting vascular dysfunction. Histopathology 77: 198–209, 2020 https://doi.org/10.1111/his.14134
46. Shetty AA, Tawhari I, Safar-Boueri L, Seif N, Alahmadi A, Gargiulo R, Aggarwal V, Usman I, Kisselev S, Gharavi AG, Kanwar Y, Quaggin SE: COVID-19-Associated glomerular disease. J Am Soc Nephrol 32: 33–40, 2021
47. Hadjadj J, Yatim N, Barnabei L, Corneau A, Boussier J, Smith N, Péré H, Charbit B, Bondet V, Chenevier-Gobeaux C, Breillat P, Carlier N, Gauzit R, Morbieu C, Pène F, Marin N, Roche N, Szwebel T-A, Merkling SH, Treluyer J-M, Veyer D, Mouthon L, Blanc C, Tharaux P-L, Rozenberg F, Fischer A, Duffy D, Rieux-Laucat F, Kernéis S, Terrier B: Impaired type I interferon activity and inflammatory responses in severe COVID-19 patients. Science 369: 718–724, 2020 https://doi.org/10.1126/science.abc6027
48. Sharma P, Uppal NN, Wanchoo R, Shah HH, Yang Y, Parikh R, Khanin Y, Madireddy V, Larsen CP, Jhaveri KD, Bijol V; Northwell Nephrology COVID-19 Research Consortium: COVID-19-Associated kidney injury: A case series of kidney biopsy findings. J Am Soc Nephrol 31: 1948–1958, 2020 https://doi.org/10.1681/ASN.2020050699
49. Bradley BT, Maioli H, Johnston R, Chaudhry I, Fink SL, Xu H, Najafian B, Deutsch G, Lacy JM, Williams T, Yarid N, Marshall DA: Histopathology and ultrastructural findings of fatal COVID-19 infections in Washington state: A case series. Lancet 396: 320–332, 2020 https://doi.org/10.1016/S0140-6736(20)31305-2
50. Golmai P, Larsen CP, DeVita MV, Wahl SJ, Weins A, Rennke HG, Bijol V, Rosenstock JL: Histopathologic and ultrastructural findings in postmortem kidney biopsy material in 12 patients with AKI and COVID-19. J Am Soc Nephrol 31: 1944–1947, 2020 https://doi.org/10.1681/ASN.2020050683
51. Santoriello D, Khairallah P, Bomback AS, Xu K, Kudose S, Batal I, Barasch J, Radhakrishnan J, D'Agati V, Markowitz G: Postmortem kidney pathology findings in patients with COVID-19. J Am Soc Nephrol 31: 2158–2167, 2020 https://doi.org/10.1681/ASN.2020050744
52. Sun J, Tang X, Bai R, Liang C, Zeng L, Lin H, Yuan R, Zhou P, Huang X, Xiong Q, Peng J, Cui F, Ke B, Su J, Liu Z, Lu J, Tian J, Sun R, Ke C: The kinetics of viral load and antibodies to SARS-CoV-2. Clin Microbiol Infect 26: 1690.e1–1690.e4, 2020 https://doi.org/10.1016/j.cmi.2020.08.043
53. Chen X, Zhao B, Qu Y, Chen Y, Xiong J, Feng Y, Men D, Huang Q, Liu Y, Yang B, Ding J, Li F: Detectable serum severe acute respiratory syndrome coronavirus 2 viral load (RNAemia) is closely correlated with drastically elevated interleukin 6 level in critically ill patients with coronavirus disease 2019. Clin Infect Dis 71: 1937–1942, 2020 https://doi.org/10.1093/cid/ciaa449
54. Muranyi W, Bahr U, Zeier M, van der Woude FJ: Hantavirus infection. J Am Soc Nephrol 16: 3669–3679, 2005 https://doi.org/10.1681/ASN.2005050561
55. Ysebaert DK, De Greef KE, De Beuf A, Van Rompay AR, Vercauteren S, Persy VP, De Broe ME: T cells as mediators in renal ischemia/reperfusion injury. Kidney Int 66: 491–496, 2004 https://doi.org/10.1111/j.1523-1755.2004.761_4.x
56. Kocovski L, Duflou J: Can renal acute tubular necrosis be differentiated from autolysis at autopsy? J Forensic Sci 54: 439–442, 2009 https://doi.org/10.1111/j.1556-4029.2008.00956.x

**Received:** November 20, 2020 **Accepted:** February 11, 2021

A.B., P.E., and S.G. contributed equally to this work.